



Pyrolysis and its mechanism of organomontmorillonite (OMMT) influenced by different functional groups

Liangliang Zhang¹ · Jinzhen Cao¹

Received: 19 June 2018 / Accepted: 23 November 2018 / Published online: 30 November 2018
© Akadémiai Kiadó, Budapest, Hungary 2018

Abstract

In this study, three types of long-chain surfactants including 12-aminododecanoic acid (ADA), hexadecyl trimethyl ammonium bromide (CTAB) and sodium laurylsulfonate (SLS) were intercalated into Na-montmorillonite layers through ion exchange, resulting increased basal spacing of the interlayers, as well as the change of clay surface from hydrophilic to hydrophobic as proved by X-ray diffraction and Fourier transform infrared spectroscopy analyses. Differential thermal analysis, thermogravimetric measurement combined with infrared spectroscopy and derivative thermogravimetric analysis were used to understand the relation between the thermal stability and the molecular structure of the organo-modified montmorillonites. The results showed that MMT increased the decomposition temperature of ADA, delayed the decomposition temperature of CTAB and SLS, and stimulated the generation of CO₂. The interlayer space might play a more significant role than the external surface of MMT in influencing the pyrolysis of OMMT.

Keywords Montmorillonite (MMT) · Modification · Thermal stability · Molecular structure · Pyrolysis

Introduction

Montmorillonite (MMT), which presents high aspect ratio, ion exchange and good mechanical strength, has been modified as host materials for surfactants and, as such, has been dispersed into polymeric matrix in order to improve the thermal properties and moisture resistance [9, 10, 17, 38]. MMT has a kind of sandwiched structure composed of alumina octahedral sheet between two silica tetrahedral sheets, connected by oxygen atoms common to the both sheets [1, 36]. The thickness of each layer is about 1 nm, and the lateral dimension may vary from 30 nm to several microns or larger, resulting in high aspect ratio and specific surface area [27, 30]. Based on the nano effect, MMT has been used to reinforce polymer composites effectively even at very low amount [25]. However, due to isomorphic substitutions in the lattice, the MMT layer is usually negatively charged, which is counterbalanced by

exchangeable cations like Na⁺, Ca²⁺ and Li⁺ [28]. As a result, natural MMT is hydrophilic and tends to form agglomerates. The well dispersion of unmodified MMT in nonpolar polymers is much too difficult, which restricts enhancement of the polymer properties to some extent [6].

To overcome this restriction, the normally hydrophilic silicate surface should be converted to organophilic by ion-exchange reactions with some organic compounds, including cationic, anionic surfactants, or organic acid [7, 22, 29, 41]. Usually, alkylammonium salts are used to modify montmorillonite, producing clay with a hydrophobic character and a greater interlayer space [16]. However, due to the degradation of alkylammonium salts themselves at elevated temperatures, the instability of the organomontmorillonite (OMMT) would adversely affect the stability of the nanocomposites [34]. Moreover, it has been reported that anionic surfactants are capable of intercalating MMT, but the driving force to assist them to adsorb and intercalate in MMT is limited, which poses difficulty in this process [40]. Cationic and anionic surfactant mixtures, such as hexadecyl trimethyl ammonium bromide (CTAB) and sodium dodecyl sulfonate (SDS) blend, have also been used as modifiers to synthesize cation–anion OMMT. It was demonstrated that anionic

✉ Jinzhen Cao
caoj@bjfu.edu.cn

¹ College of Materials Science and Technology, Beijing Forestry University, Qinghua East Road 35, Haidian, Beijing 100083, China

surfactant can be intercalated into MMT more easily through the interaction with cationic surfactant rather than by ion exchange [11, 12, 41]. As for organic acid modifier, ADA in the MMT undergone Hoffman elimination and hydrocracking during the heating process and produced NH_3 and saturated hydrocarbons [24]. Liu et al. [23] found that organic modifiers with different functional groups in the presence of MMT exhibited varying pyrolysis behaviors. However, less attention was put on the relationship between the thermal stability and the molecular structure of the organo-modified montmorillonites.

Herein, the objective of our study is to investigate the effects of three different modifiers including a cationic surfactant (hexadecyl trimethyl ammonium bromide, CTAB), an anionic surfactant (sodium laurylsulfonate, SLS) and an organic acid surfactant (12-aminododecanoic acid, ADA) on structure and thermal degradation of OMMT. These modifiers have all been previously used in MMT modification [8, 19, 30] and proved to be able to intercalate into MMT layers. Their molecular structures are shown in Table 1. CTAB contains alkyl quaternary ammonium cations, SLS is characterized with alkyl sulfo anions, and ADA contains amino in one end and carboxyl group in the other end. These three modifiers contain similar length of alkyl chains but different functional groups, therefore, can be used to study the effect of functional groups on pyrolysis of OMMT.

In this study, X-ray diffraction (XRD) and Fourier transform infrared spectroscopy (FTIR) were used to characterize OMMT prepared by different modifiers, and

derivative thermogravimetric analysis (DTG) and thermogravimetric measurement combined with Fourier transform infrared spectroscopy (TG-FTIR) were used to investigate the thermal degradation performance of these OMMT.

Materials and methods

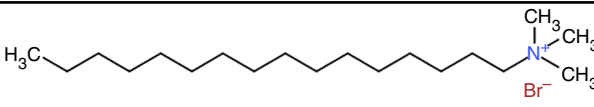
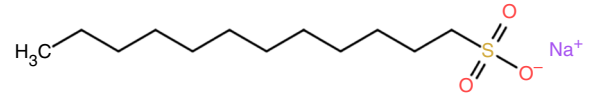
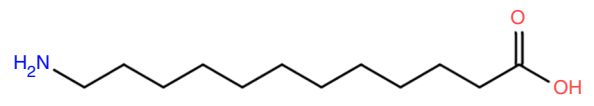
Chemical agents

Na-montmorillonite (Na-MMT) (Nanocor Inc., USA) was purchased from East West Company, Beijing, China. The specific gravity is 2.6. The mean particle size is around 16–22 μm . The pH of 5%w/w Na-MMT in distilled water is 9–10. The aspect ratio (length/width) is 150–200, and the cation exchange capacity (CEC) is 145 mmol/100 g. CTAB (AR) was provided by Shanghai Macklin Biochemical Co., Ltd. of China. SLS (AR) was provided by Xilong Chemical Co., Ltd. of China. ADA (AR) was provided by J&K Scientific Ltd., China. The modified montmorillonites were, respectively, denoted as CTAB-MMT, SLS-MMT and ADA-MMT.

Preparation of OMMT

First, the Na-MMT was dried in an oven at 60 $^{\circ}\text{C}$ for 24 h to remove water attached on its surface. 10 g of MMT was dispersed in 200 mL distilled water at 80 $^{\circ}\text{C}$ for 24 h under magnetic stirring, and then subjected to sonicating with an ultrasound processor (KQ-250DB, Kun Shan Ultrasonic

Table 1 Organic modifiers used in this study

Name	Type	Molecular structure	Mw/g mol ⁻¹
Hexadecyl trimethyl ammonium bromide	Cationic	$\text{CH}_3(\text{CH}_2)_{15}\text{N}(\text{CH}_3)_3\text{Br}$ 	364.45
Sodium laurylsulfonate	Anionic	$\text{CH}_3(\text{CH}_2)_{11}\text{SO}_3\text{Na}$ 	272.38
12-Aminododecanoic acid	Organic acid	$\text{NH}_2(\text{CH}_2)_{11}\text{COOH}$ 	215.33

Instruments Co., Ltd., China) for 30 min at nominal power of 40% amplitude and full cycle. 14.5 mmol CTAB was added slowly to 100 mL of ethanol solution (ethanol: distilled water = 1:1) and 0.5 N HCl. The treated Na-MMT and CTAB were placed in a three-necked flask and stirred at 80 °C for another 24 h. The resultant mixture obtained is filtered and repeatedly washed with large amount of distilled water until no white precipitate is detected using an AgNO₃ solution. Then it is dried in an oven at 80 °C for 24 h and ground to powder. Finally, it is screened via a 200-mesh sieve and stored in brown glass bottle. Other sets of organoclay were prepared in a similar way using SLS and ADA as modifiers, respectively.

Characterization and thermal analyses

X-ray diffraction (XRD) analysis of the samples was recorded on a diffractometer (D8 Advance, Bruker, Germany) with Ni filter and Cu K α radiation ($\lambda = 0.154$) operated at a generator voltage of 40 kV and a generator current of 30 mA. A diffraction angle of 2θ ranging from 1° to 10° with a scanning rate of 2° min⁻¹ was used in this study considering that the 2θ of Na-MMT and OMMT assigned to [001] reflection usually display within this range. The d_{001} data were then calculated by Bragg equation shown below:

$$2d \sin \theta = n\lambda \quad (1)$$

where d corresponds to the spacing between the diffraction lattice planes, θ is the diffraction angle and λ is the wavelength of the X-ray ($\lambda = 1.5405$ Å).

The FTIR spectroscopy was performed within the range of 400–4000 cm⁻¹ on a Nicolet 6700 spectrometer (Thermo Fisher Scientific, USA) using the attenuated total reflection infrared (ATR). All the spectra were obtained by averaging of 32 scans at a resolution of 4 cm⁻¹.

The TG-FTIR analysis was performed on a thermogravimetric analyzer (Q5000IR, TA instruments, USA) coupled with a Fourier transform infrared spectroscopy (VERTEX 70, Bruker, Germany). Approximately, 50 mg of sample was heated from room temperature (25 °C) to 1000 °C under a steady nitrogen (N₂) flow rate of 50 mL min⁻¹ at a temperature ramp rate of 10 °C min⁻¹. The volatiles released from samples would be swept into FTIR gas cell quickly by pure N₂. And then absorbance information was obtained at different wavenumber as a function of temperature. The FTIR spectrometer recorded spectra in the range of 400–4000 cm⁻¹ and the resolution factor was collected at 1 cm⁻¹.

TGA/DTG curves of samples were obtained on a STA 449 F3 thermoanalyzer (Netzsch, Germany) under dynamic nitrogen atmosphere (50 mL min⁻¹) using a platinum

crucible at a heating rate of 10 °C min⁻¹ from room temperature (25 °C) to 900 °C.

Results and discussion

Interlayer spacing in OMMT with different functional groups

The basal spacing between the clay platelets was revealed by XRD analysis. The XRD diffraction patterns of Na-MMT, CTAB-MMT, SLS-MMT and ADA-MMT are illustrated in Fig. 1 and the interlayer spacing data are listed in Table 2.

The XRD pattern of Na-MMT displays a peak around $2\theta = 6.8^\circ$ which is assigned to [001] reflection and d_{001} is 1.30 nm, suggesting that the platelets in Na-MMT are very close to each other and difficult to be separated. After modification with ADA, CTAB and SLS, the interlayer spacing increased to different extents by the intercalation of these modifier molecules.

This reflection shifted to $2\theta = 5.08^\circ$ in the spectrum of ADA-MMT, and the corresponding basal plane spacing was calculated as $d_{001} = 1.74$ nm, suggesting that the long alkyl groups intercalated into the silicate galleries (Fig. 1d and Table 2).

The [001] reflection was observed at $2\theta = 4.00^\circ$ ($d_{001} = 2.21$ nm) in the spectrum of CTAB-MMT, resulting in a 0.91 nm expansion of the basal spacing (Fig. 1b and Table 2). The intercalated CTAB most probably adopted a paraffin type in the interlayer of MMT [39]. In this type of intercalation, the ammonium groups remain attached to the silicate layer and the chains in all-trans conformation point away from the surface [5].

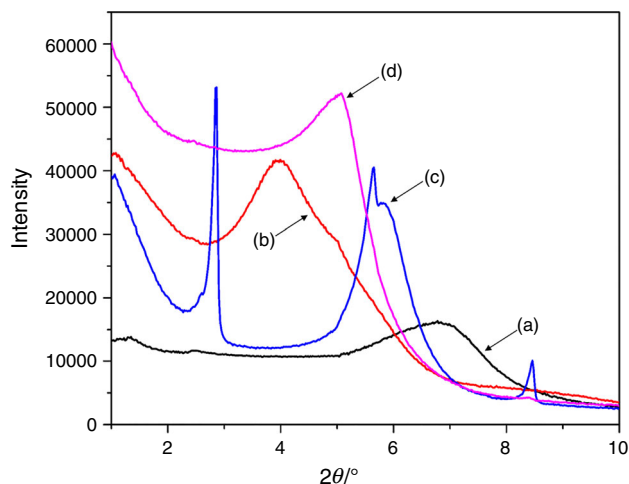


Fig. 1 XRD diffraction patterns of a Na-MMT, b CTAB-MMT, c SLS-MMT and d ADA-MMT

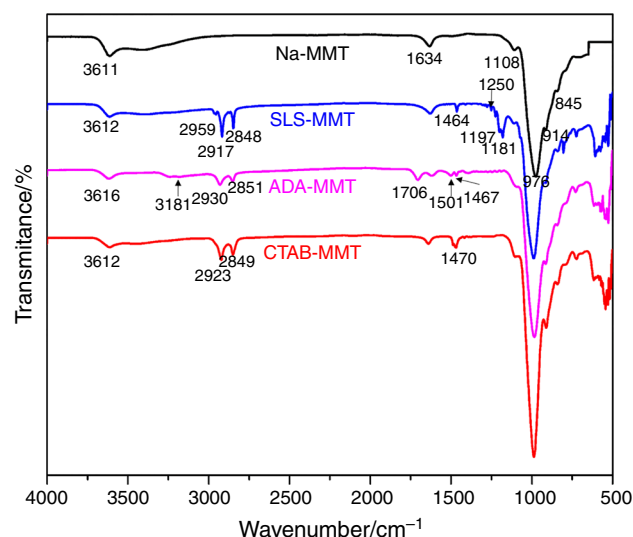
Table 2 Interlayer spacing of Na-MMT, SLS-MMT, ADA-MMT and CTAB-MMT

	$2\theta/^\circ$	d_{001}/nm
Na-MMT	6.78	1.30
CTAB-MMT	4.00	2.21
SLS-MMT	2.86	3.08
	5.65	1.56
	8.46	1.05
ADA-MMT	5.08	1.74

The distribution of interlayer spacing of platelets in SLS-MMT was characterized by three prominent reflections appeared at $2\theta = 2.86^\circ$, 5.65° and 8.46° , corresponding to d_{001} of 3.08 nm, 1.56 nm and 1.05 nm, respectively (Fig. 1c and Table 2). In neutral solution, it is difficult for anion $\text{C}_{12}\text{H}_{25}\text{SO}_3^-$ with negative charge to intercalate into the silicate galleries [40]. However, at relatively low pH values, parts of the SLS anions would be protonated and may enter the interlayer space until $\text{C}_{12}\text{H}_{25}\text{SO}_3\text{H}$ reaches balance between the dispersion and interlayer space, thus increasing the spacing of MMT to varying degrees. Moreover, the anionic surfactant could enter the interlayer space as ion pairs with H_3O^+ or Na^+ and Ca^{2+} as counter ions [13, 31]. While, cationic surfactant, such as CTAB, could intercalate into MMT more easily by van der Waals force between hydrocarbon chains and electrostatic repulsion between the hydrophilic heads of the surfactant [11, 26]. The different modification mechanisms between cationic and anionic surfactants cause uneven distribution of the anionic surfactant in the silicate galleries. Therefore, the XRD pattern of SLS-MMT displays two peaks at 2.86° and 5.65° even a shoulder between 5.6° and 6.0° , which is consistent with the previous studies [12, 40, 43]. Furthermore, when excess acid is used, the Na^+ ions could be exchanged by H^+ ions instead of the SLS anions and thus decrease the spacing of MMT [14].

Characterization by FTIR analyses

The FTIR spectra of Na-MMT, ADA-MMT, CTAB-MMT and SLS-MMT are illustrated in Fig. 2. The bands appeared at 3611 cm^{-1} and 1634 cm^{-1} are assigned to the asymmetric stretching vibration of the structural $-\text{OH}$ groups and the bending-in-plan vibration of $\text{H}-\text{O}-\text{H}$, respectively [3]. The characteristic bands of Na-MMT are detected at 1108 cm^{-1} due to out-of-plane Si-O stretching vibrations, 976 cm^{-1} related to in-plane Si-O stretching vibration, and bands at 914 cm^{-1} , 845 cm^{-1} associated with Al-Al-OH and Al-Mg-OH bending vibration, respectively [2]. Upon modification, their relative positions remain nearly invariable, indicating that the main bones of MMT did not change with the modification [8]. The FTIR

**Fig. 2** FTIR spectra of Na-MMT and OMMT modified by different modifiers

spectra of OMMT exhibit two additional peaks within the range of $2800\text{--}3000\text{ cm}^{-1}$, which can be attributed to the CH_2 asymmetric stretching and the symmetric stretching of intercalated modifiers with the silicate layer [32].

For pure ADA, two intense bands near 1514 cm^{-1} and 1396 cm^{-1} correspond to the symmetric and asymmetric $\text{R}-\text{COO}^-$ stretching, respectively [24]. However, in the spectra of ADA-MMT, two bands of $\text{R}-\text{COO}^-$ at 1501 cm^{-1} and 1467 cm^{-1} are much weaker than those of ADA, and a new band at 1706 cm^{-1} appears responding to the $\text{C}=\text{O}$ stretching vibration in non-ionized carboxyl groups. During the synthesis of ADA-MMT, when HCl was added to the aqueous solution of ADA, distilled water and Na-MMT, parts of the COO^- anions are protonated into COOH by H^+ and form $\text{C}=\text{O}$ band in ADA-MMT [19]. Besides, the ionic bonded $\text{N}-\text{H}$ stretching band of $-\text{NH}_2$ at 3181 cm^{-1} appears in the spectrum as well.

The absorption peaks from CTAB for CTAB-MMT can be found at 2923 and 2849 cm^{-1} arising from the stretching of CH_2- and 1470 cm^{-1} arising from $\text{N}-\text{H}$ bending vibrations [22], confirming the alkyl ammonium in the interlayer galleries of the clay.

The spectra of SLS-MMT show the characteristic absorption bands of CH_3- and CH_2- groups at 2959 , 2917 , 2848 and 1464 cm^{-1} and the sulfonic acid group at 1181 cm^{-1} [40]. In particular, the characteristic absorption peak of SLS-MMT at 1250 cm^{-1} and 1197 cm^{-1} are corresponding to symmetric stretch of $\text{S}=\text{O}$, indicating that interactions between the SLS and the mineral interlayer [42].

TG-FTIR characterization of the pyrolysis of OMMT

Thermogravimetric analysis of Na-MMT and OMMT modified by different modifiers

Figure 3 displays the TG curves and the corresponding derivative curves (DTG) for Na-MMT, ADA, ADA-MMT, CTAB, CTAB-MMT, SLS and SLS-MMT, respectively. Two decomposition steps can be observed in the TG–DTG curve of Na-MMT (Fig. 3a). The first step occurs below 200 °C with a sharp peak DTG at 114 °C and shows a mass loss of 4.35%, which corresponds to the elimination of adsorbed water on surface or interlayer water. The second step in the range 500–700 °C with a mass loss of approximately 3.81% corresponds to the dehydroxylation of the silicate lattice, in which a broad DTG peak occurs at 626 °C [18, 23, 24, 37].

Pure ADA begins to decompose after 200 °C with a weak DTG peak at 211 °C mainly responding to the loss of water (Fig. 3b). The major thermal events of pure ADA occur in the range of 400–500 °C and result in a sharp DTG peak at 465 °C, which is attributed to the loss of minor products, such as CO₂, N-containing compounds and carboxylic acid. Values of these peaks associated with the pyrolysis of ADA have been well studied by several research groups [21, 23]. As shown in Fig. 3c, the thermal events of ADA-MMT that occurring below 200 °C are attributed to the dehydration of the free water and residual interlayer water. Compared with the free water mass loss of 4.35% for Na-MMT, the water content is only 1.88% for ADA-MMT, implying the hydrated sodium cations have been replaced by ADA. The mass loss of ADA-MMT in the range of 200–500 °C is 20.02%, which indicated the initial content of ADA in ADA-MMT. Two overlapping peaks sourced from the degradation of organic matter could be observed at 328 °C and 362 °C, which are obviously lower than the corresponding temperatures of ALA (at about 130 °C).

Compared with Na-MMT, the TG curve of CTAB-MMT in the stage of dehydration (50–200 °C) is much milder (Fig. 3e). And the mass loss associated with free water for CTAB-MMT below 200 °C is only 1.6%, implying that the hydrated sodium cations have been replaced by CTAB. In Fig. 3d, e, the main DTG peaks of organics in CTAB and CTAB-MMT appear at 271 and 297 °C, respectively. The weak DTG peak of CTAB-MMT at 422 °C indicated that a little CTAB had entered into the silicate lattice. These shoulder peaks of CTAB-MMT in Fig. 3e were both remarkably higher than that of CTAB (271 °C), indicating that the lamellar structure of MMT delayed the pyrolysis of CTAB. In addition, the pyrolysis

products of CTAB were mainly the generation of aliphatic hydrocarbons and trimethylamine ((CH₃)₃N).

In Fig. 3f, SLS compound exhibits a main DTG peak at 430 °C and a residual rate about 19.56% after 700 °C, indicating the sodium and sulfur contents in SLS has not decomposed under N₂ atmosphere. As shown in Fig. 3g, the DTG curve of SLS-MMT displays two peaks at 124 and 475 °C, corresponding to the release of physically absorbed water and the degradation of the intercalated SLS, respectively. The main gaseous products released at 475 °C were carbon dioxide (2359 and 2339 cm⁻¹) and hydrocarbons (2966, 2935 and 2879 cm⁻¹), which were similar to SLS and SLS-MMT (Figs. 4c, 5c). The maximum degradation temperatures of pure SLS were slightly lower than of SLS-MMT, which implied that intercalation delayed the pyrolysis of SLS. This interesting phenomenon indicated that the pyrolysis temperature of SLS within the interlayer of MMT was mainly affected by the barrier effect of MMT sheets in consideration of the weak association between SLS and MMT. The initial pyrolysis products of SLS were trapped within the confined interlayer spaces, and thus the maximum rate temperature occurred at a higher temperature than pure SLS [4, 37].

Pyrolytic behavior of OMMT modified by different modifiers

The 3D-FTIR spectra of the evolved gases of OMMT modified by different modifiers are shown in Fig. 4, and the corresponding FTIR spectra at different temperatures are presented in Fig. 5. For ADA-MMT, the free water and interlayer water were detected below 200 °C, which were strongly confirmed by the signal associated with gaseous water (1300–2000 cm⁻¹ and 3500–4000 cm⁻¹) (Fig. 5a). Two new bands were detected, indicating that ADA underwent decarboxylation processes at elevated temperatures. Within the range of 200–500 °C, the emerged bands of aliphatic hydrocarbons (2965, 2935, 2877, 1465 and 1382 cm⁻¹) and NH₃ (966 and 931 cm⁻¹) were found (Figs. 4a, 5a) [35]. The phenomenon that the characteristic bands of CO₂ (2366 and 2331 cm⁻¹) always existed with the temperature increasing attracted our attention. Below 200 °C, the signals of CO₂ and water were detected (Figs. 4a, 5a), indicating that ADA began to dehydrate and decarboxylate. Within the range of 200–500 °C, the decarboxylation reaction continued (Figs. 4a, 5a), which is different from previous literature [24]. At higher temperatures, the production of CO₂ may be due to the reaction between the residue and the oxygen in the crystal structure of MMT.

For CTAB-MMT, the main gaseous products that evolved from CTAB released at 422 °C were mainly aliphatic hydrocarbons (2968, 2933 and 2866 cm⁻¹), CO₂ (2358 and 2332 cm⁻¹), NH₃ (966 and 930 cm⁻¹) and HCN

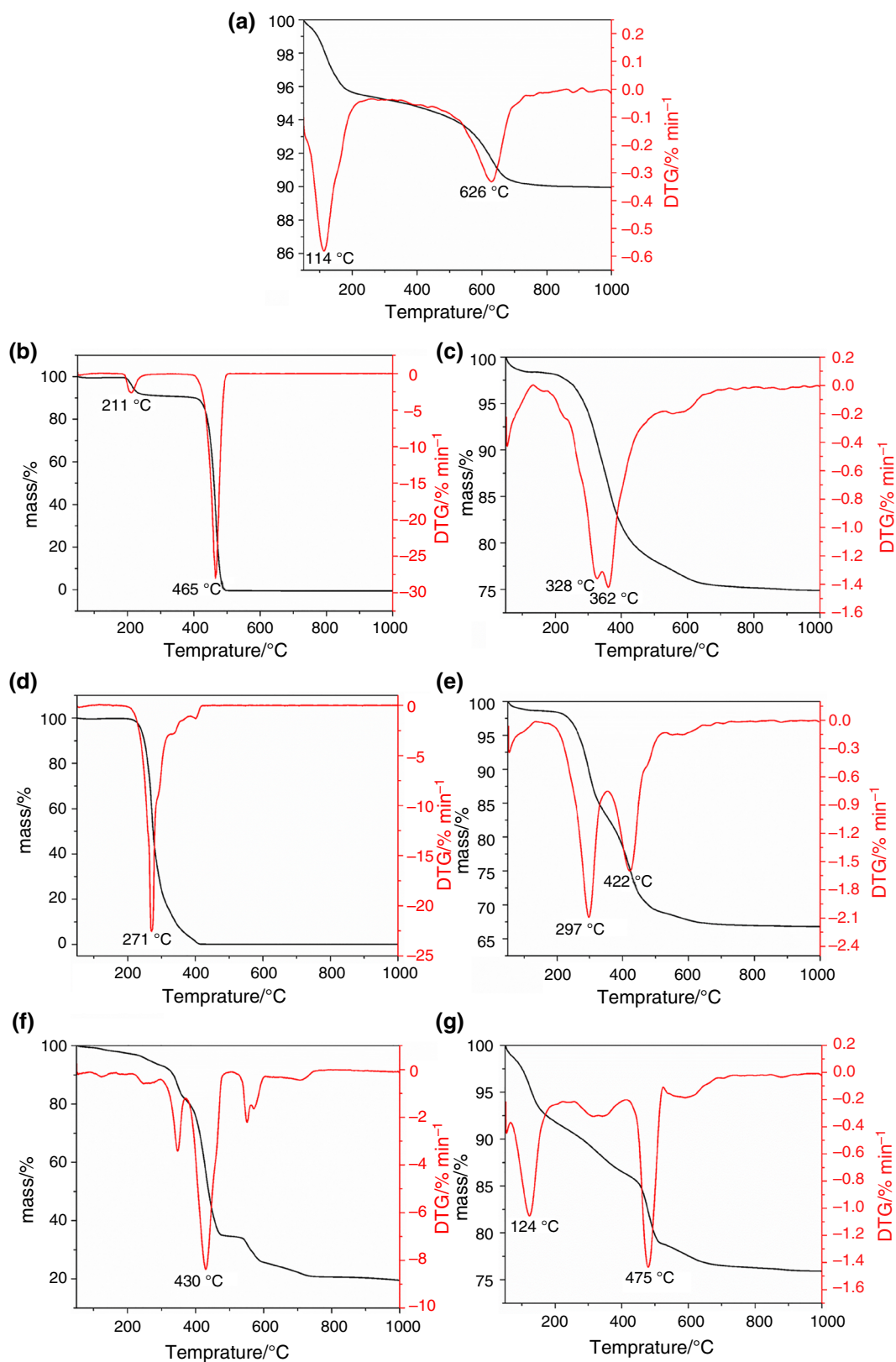


Fig. 3 TG-DTG curves of Na-MMT (a), ADA (b), ADA-MMT (c), CTAB (d), CTAB-MMT (e), SLS (f) and SLS-MMT (g)

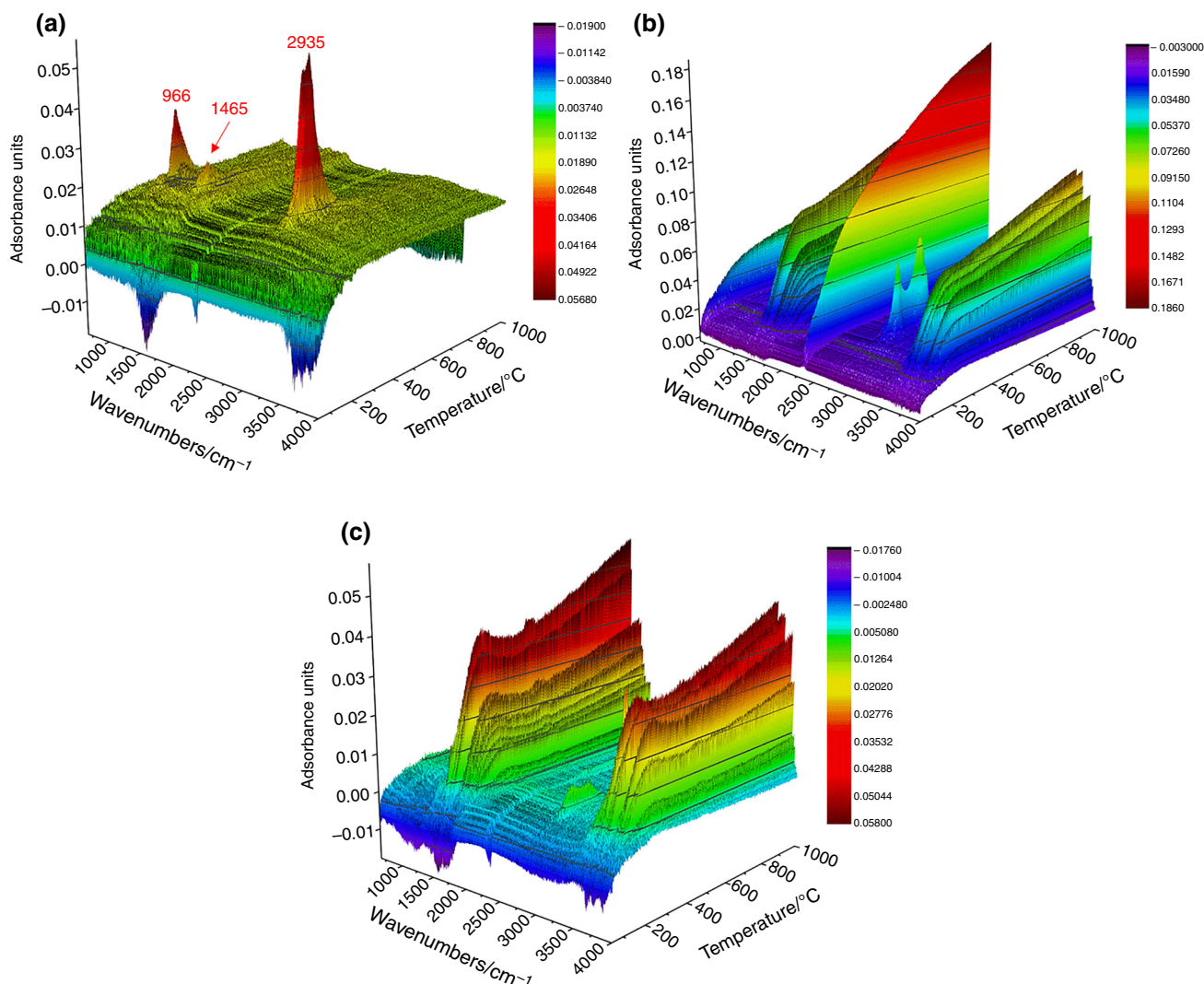


Fig. 4 3D-FTIR spectrum of ADA-MMT (a), CTAB-MMT (b) and SLS-MMT (c)

(719 cm^{-1}) (Figs. 4b, 5b). The spectrum obtained at 500 °C showed the bands corresponding to aliphatic hydrocarbons practically disappeared, which confirmed the TG result that there is no pyrolysate after 500 °C. In addition, the bands of CH-stretching (2823 and 2775 cm^{-1}) and CN-stretching (1034 cm^{-1}) proved the generation of trimethylamine ((CH_3)₃N).

For SLS-MMT, a weak peak at 3000–2800 cm^{-1} can be observed at early degradation. Then, the peak disappeared quickly. After that, FTIR spectra of evolved gases at 475 °C indicate that the production of carbon dioxide (2359 and 2339 cm^{-1}) and hydrocarbons (2966, 2935 and 2879 cm^{-1}) reached the maximum degradation rate (Figs. 4c, 5c).

Pyrolysis mechanism of OMMT modified by different modifiers

For ADA-MMT (Figs. 4a, 5a), it was obvious that the thermal decomposition products occurred in the following order: CO_2 , hydrocarbons and NH_3 , which corresponded to the pyrolysis of $-\text{COOH}$, carbon chain and $-\text{NH}_2$, respectively. Therefore, the first pyrolytic reaction step was decarboxylation, then followed by carbon chain cleavage and deamination [23].

Consequently, decarboxylation and deamination were two main important reactions of ADA with carboxyl groups and amine that occurred in the presence of OMMT. The Lewis acid sites of MMT (the acceptor of electrons pair) catalyzed the decarboxylation and promoted the generation of CO_2 , which resulted from Al^{3+} , Fe^{3+} exposed at the edges of the clay minerals and the hydrated

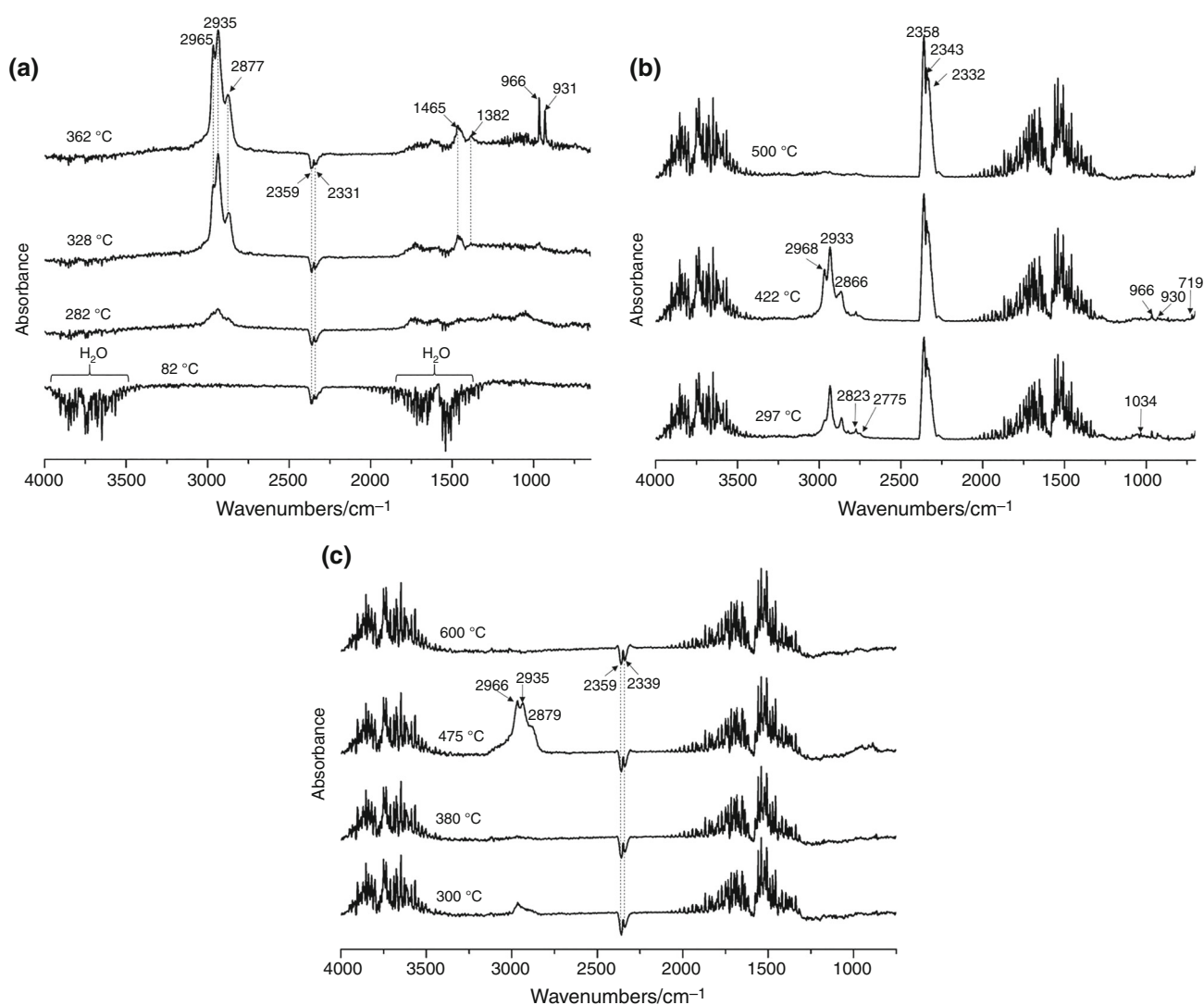


Fig. 5 FTIR spectra of ADA-MMT (a), CTAB-MMT (b) and SLS-MMT (c) at different degradation temperatures

cations after dehydrating [33]. The Brønsted acid sites of MMT strongly promoted the deamination reaction via Hofmann elimination pathway [20]. The aliphatic hydrocarbons and NH_3 released suggested Hofmann elimination occurred. However, in this study, there is no evidence that unsaturated alkyl products have been detected in the case of ADA-MMT. Compared with the ADA on the external surface of MMT, the organic modifier pyrolysis among the layers was confined by the clay sheets and was catalyzed from alkene to alkane.

For CTAB-MMT, it has been reported that nucleophilic substitution reaction and Hoffmann elimination was the main reactions of CTAB in the presence of OMMT [37]. In previous studies [15], during the pyrolysis of pure CTAB, it was detected that the yield of bromomethane (CH_3Br) and alkane was higher than that of hydrogen bromide (HBr) and alkene, indicating the nucleophilic substitution was the

main reaction. After mixing with MMT, the signal of trimethylamine was observed with the bromomethane and hydrogen bromide [37]. It is probable that the Brønsted acid sites sourced from interlayer space promoted the pyrolysis of CTAB cations and produced trimethylamine through Hoffmann elimination.

Elimination reaction seems to predominate at elevated temperatures in the degradation of SLS-MMT. However, alkene was not found during the pyrolysis of SLS-MMT, which can be explained similar to that of ADA-MMT.

Conclusions

In this study, OMMT were synthesized by using three types of organic modifiers with different functional groups. The functionalization was confirmed by XRD and FTIR results.

It was concluded that these organic modifiers were all intercalated into the interlayers of MMT to different extents and transformed clay surface from hydrophilicity to hydrophobicity. Both cationic surfactant and organic acid showed single basal d-spacing, and therefore are more homogeneous than anionic surfactant in clay sheet distribution. The interlayer structure of MMT had significant effects on the pyrolysis of OMMT. The pyrolytic behavior of organic modifiers was related to the functional group and the structures of MMT. As illustrated in TGA-DTG and TG-FTIR, MMT accelerated the pyrolysis of ADA with carboxyl and amino groups but delayed the pyrolysis of CTAB with quaternary ammonium cation and SLS with sulfo anion. Due to the steric hindrance and abundance in solid acid sites, interlayer space might play a more significant role than the external surface of MMT in influencing the pyrolysis of OMMT. The solid acid sites not only catalyzed the decarboxylation and promoted the generation of CO₂ but also promoted the Hoffmann elimination reaction. This study indicates that when adding OMMT to heat-resistant composites, it is necessary to consider the influence of organic modifiers with different functional groups.

Acknowledgements This work was financially supported by the National Key Research and Development Program of China (2017YFD0600203).

References

- Ahmed L, Zhang B, Shen RQ, Agnew RJ, Park H, Cheng ZD, Mannan MS, Wang QS. Fire reaction properties of polystyrene-based nanocomposites using nanosilica and nanoclay as additives in cone calorimeter test. *J Therm Anal Calorim.* 2018;132:1853–65.
- Alves JL, Vieira e Rosa PdT, Morales AR. Evaluation of organic modification of montmorillonite with ionic and nonionic surfactants. *Appl Clay Sci.* 2017;150:23–33.
- Amarasinghe PM, Katti KS, Katti DR. Nature of organic fluid-montmorillonite interactions: an FTIR spectroscopic study. *J Colloid Interface Sci.* 2009;337:97–105.
- Bellucci F, Camino G, Frache A, Saffa A. Catalytic charring-volatilization competition in organoclay nanocomposites. *Polym Degrad Stab.* 2007;92:425–36.
- Bonczek JL, Harris W, Nkedi-Kizza P. Monolayer to bilayer transitional arrangements of hexadecyltrimethylammonium cations on Na-montmorillonite. *Clays Clay Miner.* 2002;50:11–7.
- Bromberg L, Straut CM, Centrone A, Wilusz E, Hatton TA. Montmorillonite functionalized with pralidoxime as a material for chemical protection against organophosphorous compounds. *ACS Appl Mater Interfaces.* 2011;3:1479–84.
- Bu H, Yuan P, Liu H, Liu D, Zhou X. Thermal decomposition of long-chain fatty acids and its derivative in the presence of montmorillonite. *J Therm Anal Calorim.* 2017;128:1661–9.
- Cai X, Tan S, Liao M, Wu T, Liu R, Yu B. Thermal stability and long-acting antibacterial activity of phosphonium montmorillonites. *J Cent South Univ Technol.* 2010;17:485–91.
- Campos LMP, Boaro LC, Santos TMR, Santos VJ, Grecco-Romano R, Santos MJ, Parra DF. Polymerization shrinkage evaluation in experimental dental composite filled with montmorillonite nanoparticles. *J Therm Anal Calorim.* 2018;131:771–4.
- Carrasco F, Perez-Maqueda LA, Santana OO, MasPOCH ML. Enhanced general analytical equation for the kinetics of the thermal degradation of poly(lactic acid)/montmorillonite nanocomposites driven by random scission. *Polym Degrad Stab.* 2014;101:52–9.
- Chen D, Chen J, Luan X, Ji H, Xia Z. Characterization of anionic surfactants modified montmorillonite and its application for the removal of methyl orange. *Chem Eng J.* 2011;171:1150–8.
- Chen D, Zhu JX, Yuan P, Yang SJ, Chen TH, He HP. Preparation and characterization of anion-cation surfactants modified montmorillonite. *J Therm Anal Calorim.* 2008;94:841–8.
- Chen DM, Chen J, Wang XM, Luan XL, Ji HP, Xu F. Adsorption of methylene blue from aqueous solution by anionic surfactant modified montmorillonite. *Adv Mater Res.* 2011;178:29–34.
- Chen HH, Thirumavalavan M, Ma YJ, Lee JF. The influence of structural and processing parameters of modifiers on the interlayer structure of modified montmorillonite. *RSC Adv.* 2015;5:83217–24.
- Davis RD, Gilman JW, Sutto TW, Callahan JH, Trulove PC, De Long H. Improved thermal stability of organically modified layered silicates. *Clays Clay Miner.* 2004;52:171–9.
- de Paiva LB, Morales AR, Valenzuela Diaz FR. Organoclays: properties, preparation and applications. *Appl Clay Sci.* 2008;42:8–24.
- Fitaroni LB, de Lima JA, Cruz SA, Waldman WR. Thermal stability of polypropylene-montmorillonite clay nanocomposites: limitation of the thermogravimetric analysis. *Polym Degrad Stab.* 2015;111:102–8.
- He HP, Ding Z, Zhu JX, Yuan P, Xi YF, Yang D, Frost RL. Thermal characterization of surfactant-modified montmorillonites. *Clays Clay Miner.* 2005;53:287–93.
- Katti KS, Sikdar D, Katti DR, Ghosh P, Verma D. Molecular interactions in intercalated organically modified clay and clay-polycaprolactam nanocomposites: experiments and modeling. *Polymer.* 2006;47:403–14.
- Leite IF, Soares APS, Carvalho LH, Raposo CMO, Malta OML, Silva SML. Characterization of pristine and purified organobentonites. *J Therm Anal Calorim.* 2010;100:563–9.
- Li J, Liu Y, Shi J, Wang Z, Hu L, Yang X, Wang C. The investigation of thermal decomposition pathways of phenylalanine and tyrosine by TG-FTIR. *Thermochim Acta.* 2008;467:20–9.
- Lin KJ, Jeng US, Lin KF. Adsorption and intercalation processes of ionic surfactants on montmorillonite associated with their ionic charge. *Mater Chem Phys.* 2011;131:120–6.
- Liu H, Yuan P, Liu D, Bu H, Song H, Qin Z, He H. Pyrolysis behaviors of organic matter (OM) with the same alkyl main chain but different functional groups in the presence of clay minerals. *Appl Clay Sci.* 2018;153:205–16.
- Liu H, Yuan P, Qin Z, Liu D, Tan D, Zhu J, He H. Thermal degradation of organic matter in the interlayer clay-organic complex: a TG-FTIR study on a montmorillonite/12-aminolauric acid system. *Appl Clay Sci.* 2013;80–81:398–406.
- Madhoushi M, Chavooshi A, Ashori A, Ansell MP, Shakeri A. Properties of wood plastic composite panels made from waste sanding dusts and nanoclay. *J Compos Mater.* 2014;48:1661–9.
- Mao H, Li B, Li X, Yue L, Liu Z, Ma W. Novel one-step synthesis route to ordered mesoporous silica-pillared clay using cationic-anionic mixed-gallery templates. *Ind Eng Chem Res.* 2010;49:583–91.

27. Mat'ko I, Sausa O, Cechova K, Jesenak K. Study of water in Ca-montmorillonite by thermal analysis and positron annihilation lifetime spectroscopy. *J Therm Anal Calorim.* 2018;133:247–54.
28. Mittal V. Polymer layered silicate nanocomposites: a review. *Materials.* 2009;2:992–1057.
29. Puffr R, Spatova JL, Brozek J. Clay mineral/polyamide nanocomposites obtained by in situ polymerization or melt intercalation. *Appl Clay Sci.* 2013;83–84:294–9.
30. Ray SS, Okamoto M. Polymer/layered silicate nanocomposites: a review from preparation to processing. *Prog Polym Sci.* 2003;28:1539–641.
31. Rutherford DW, Chiou CT. Effect of water saturation in soil organic matter on the partition of organic compounds. *Environ Sci Technol.* 1992;26:965–70.
32. Sarkar B, Megharaj M, Xi Y, Naidu R. Structural characterisation of Arquad (R) 2HT-75 organobentonites: surface charge characteristics and environmental application. *J Hazard Mater.* 2011;195:155–61.
33. Shimizu KI, Higuchi T, Takasugi E, Hatamachi T, Kodamab T, Satsuma A. Characterization of Lewis acidity of cation-exchanged montmorillonite K-10 clay as effective heterogeneous catalyst for acetylation of alcohol. *J Mol Catal A Chem.* 2008;284:89–96.
34. Wang J, Zheng X, Hao W, Xu N, Pan X. Synthesis of hyperbranched quaternary ammonium salt and its application into montmorillonite. *Powder Technol.* 2012;221:80–9.
35. Wang Z, Lv P, Hu Y, Hu K. Thermal degradation study of intumescent flame retardants by TG and FTIR: melamine phosphate and its mixture with pentaerythritol. *J Anal Appl Pyrolysis.* 2009;86:207–14.
36. Wu LM, Liao LB, Lv GC. Influence of interlayer cations on organic intercalation of montmorillonite. *J Colloid Interface Sci.* 2015;454:1–7.
37. Xie W, Gao Z, Pan WP, Hunter D, Singh A, Vaia R. Thermal degradation chemistry of alkyl quaternary ammonium montmorillonite. *Chem Mater.* 2001;13:2979–90.
38. Xu Y, Peng H, Wang X, Su S. Comparative study of different polymerically-modified clays on curing reaction and thermal properties of epoxy resin. *Thermochim Acta.* 2011;516:13–8.
39. Zawrah MF, Khattab RM, Saad EM, Gado RA. Effect of surfactant types and their concentration on the structural characteristics of nanoclay. *Spectrochim Acta A.* 2014;122:616–23.
40. Zhang Z, Liao L, Xia Z. Ultrasound-assisted preparation and characterization of anionic surfactant modified montmorillonites. *Appl Clay Sci.* 2010;50:576–81.
41. Zhang Z, Zhang J, Liao L, Xia Z. Synergistic effect of cationic and anionic surfactants for the modification of Ca-montmorillonite. *Mater Res Bull.* 2013;48:1811–6.
42. Zheng J, Li J, Hao H, Yao K. Influence of charge density and chain length on the interaction between organic anion and montmorillonite. *J Wuhan Univ Technol.* 2013;28:6–11.
43. Zhuang G, Zhang Z, Guo J, Liao L, Zhao J. A new ball milling method to produce organo-montmorillonite from anionic and nonionic surfactants. *Appl Clay Sci.* 2015;104:18–26.